35th European Rotorcraft Forum 2009
DocumentID: 101191

HELICOPTER SLING LOAD POSITIONING

H. Brenner
(Hanno.Brenner@dlr.de)

Deutsches Zentrum für Luft- und Raumfahrt e.V. (DLR)
Institute of Flight Systems
Braunschweig, Germany

Abstract.[1] The paper at hand addresses the precise positioning control of helicopter sling loads. Due to a significant decrease in handling qualities caused by the external load, the manual load positioning can be hindered. By means of linear quadratic optimal output regulation, the helicopter position as well as the load sway are controlled in an integrated approach. The position control is part of an existing AFCS, which guarantees for the basic helicopter stability. The controllers are developed and tested on the basis of a comprehensive system simulation.

Notations

Symbols

$\boldsymbol{A}$	$[-]$	system matrix
$\boldsymbol{a}$	$[m/s^2]$	acceleration $(\dot{u}, \dot{v}, \dot{w})^T$
$\boldsymbol{B}$	$[-]$	control matrix
$\boldsymbol{C}$	$[-]$	observer matrix
c_S	$[N/m]$	sling spring constant
$\boldsymbol{D}$	$[-]$	feedthrough matrix
d_S	$[N\,s/m]$	sling damping constant
$\boldsymbol{I}$	$[kg\,m^2]$	inertia tensor
J	$[-]$	performance index
$\boldsymbol{K}_y$	$[-]$	output feedback matrix
l, w, h	$[m]$	length, width, height
m	$[kg]$	mass
$\boldsymbol{R}, \boldsymbol{S}, \boldsymbol{Q}$	$[-]$	weighting matrices
$\boldsymbol{TM}$	$[-]$	transformation matrix
$\boldsymbol{U}$	$[-]$	unit matrix
$\boldsymbol{u}$	$[-]$	system control vector
$\boldsymbol{V}$	$[m/s]$	velocity $(u, v, w)^T$
$\boldsymbol{x}$	$[-]$	system state vector
$\boldsymbol{y}$	$[-]$	system output vector
(Φ, Θ, Ψ)	$[rad]$	EULER-angles
$\boldsymbol{\omega}$	$[rad/s]$	angular rates $(p, q, r)^T$
δa	$[\%]$	cyclic lateral control ($A_{1s}\,[^\circ]$)
δb	$[\%]$	cyclic longit. control ($B_{1s}\,[^\circ]$)
δc	$[\%]$	collectiv control ($\Theta_{MR}\,[^\circ]$)
δp	$[\%]$	pedal control ($\Theta_{TR}\,[^\circ]$)

Indices

A, a	aerodynamic
AP	attachment point
C	container
CG	center of gravity
cmd	command
ctvr	control variable
cur	current
g	geodetic
H	helicopter
i	i-th sling
L	load
LH	load hook
P	pendulum
R	rod with swivel joint
S	sling
trgt	target value

Abbreviations

AFCS	automatic flight control system
OM	optical marker

1 Introduction

THE capability to transport sling loads of different goods to remote locations with poor accessibility may characterize the versatile utilizability of helicopters in particular. However, due to the presence of the sling load, the dynamic behavior of the helicopter is influenced in a way that the handling qualities are degraded. Hence, the pilot workload is increased due to the task of controlling the sling load, which implies the damping of load pendulum motions as well as the precise positioning of the attached load.

[1] Paper presented at the 35th European Rotorcraft Forum, Hamburg, Germany, Sept. 22-25, 2009

(a) approach

(b) placing

Figure 1: Precise load positioning [1]

Flight tests with a CH-53G heavy-lift helicopter carrying mobile pioneer bridges as sling loads revealed certain challenges in the precise load positioning (fig. 1) [1]: The central issue in precise load positioning is given by the fact that the pilot cannot see the load in general. Hence, the detection of offsets in the desired load position is done by onboard crew members or ground personnel giving instructions to the pilot. This procedure implies time delays until a proper correction of the position error can be executed by the pilot, which by then may not be effective anymore. The longer the positioning maneuver takes, the more the pilot workload increases, which in turn leads to false control inputs and further position errors. The dynamic influence of the sling load on the helicopter increases with the weight of the load.

In order to support the development of controllers for the precise load positioning, the overall system was modelled [2]. Both subsystems – helicopter and load – are considered as rigid bodies. The flexible slings build a multiple-strap-harness. Based on the modeling of the overall system, a comprehensive simulation was designed featuring a quasi-nonlinear CH-53 helicopter model and a nonlinear load system. The sling load model comprises different aerodynamic features. The simulation tool provides trim calculation, linearization and flight simulation. Hence, a basis for system analyses and the controller development is available.

2 System Modeling and Simulation

The modeling and simulation of the overall system *helicopter-slings-load* is supported by using MATLAB & SIMULINK®. The system is built up of the two rigid bodies and a rod in which the slings are fitted (fig. 14). The rod is connected to the helicopter's single load hook and features a swivel joint in order to allow the load to turn without twisting the slings, which could elsewise exceed the load limits of the slings. The slings are modeled as flexible cables: Hence, the cable-forces represent the constraining forces within the two-body system. Different load aerodynamics can be considered. The rigid body dynamics of the helicopter, the load and the rod is discussed in the appendix.

Aerodynamics

The aerodynamic forces and moments of the helicopter ($\boldsymbol{F}^A_{H,b}, \boldsymbol{M}^A_{H,b}$) are nonlinear functions of the helicopter motion and the atmosphere, which include the relevant multi-dimensional effects sufficiently. For the present work, linear aerodynamics of a CH-53D cargo helicopter are implemented, leading to a quasi-nonlinear description of the helicopter dynamic in (58) and (59). The derivatives are obtained from [3]: They were derived by linearization of a generic nonlinear simulation code and cover a speed range from hover up to $140\,kts$ at a helicopter gross weight of 16 tons.

For the following investigations of the performance and robustness of the positioning control, a cubic container is considered as external load, featuring an edge length of $2.4\,m$. The aerodynamic coefficients have been derived in wind tunnel tests. The polars of the static aerodynamic coefficients – which lead to a tangential, and two normal forces, and a moment – were identified in [4]. However, unsteady aerodynamic influences on the load surface are not taken into account due to the rather low frequencies of the system's motions. The resulting aerodynamic forces and moments are derived by (65) and (73).

Constraining forces

The load carrying harness consists of one or more slings, whose dynamic properties are defined by specific spring and damping constants, depending on the sling material. Due to the relative motion between helicopter and load, the slings are elongated, resulting in forces (eq. 77), which in turn generate moments (eq. 82, 83) due to the offset between the sling attachment points and the respective center of gravity (fig. 14).

The sling forces and moments as well as the aerodynamic forces and moments are added to the vectorial forces and moments in the equations of motion (58) and (59).

Automatic flight control system

In order to stabilize the basic unstable helicopter, an AFCS is implemented according to [3] (fig. 3). It superposes the pilot inputs by ±10% in cyclic and collective control, and by ±3% in pedal control; the actuator rates are limited to $100\%/s$.

In section 4, the pendulum controllers are determined on the basis of the AFCS-controlled, and thus, stable helicopter.

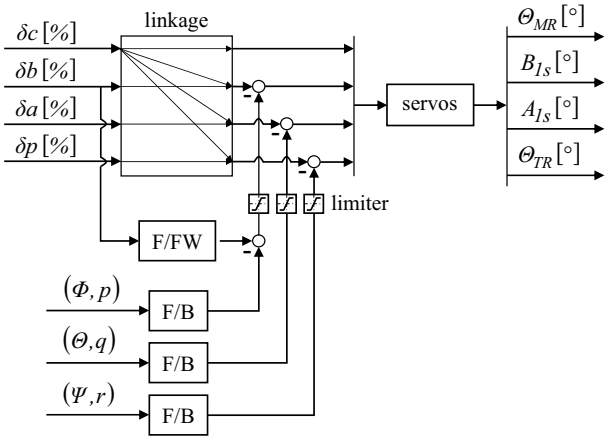

Figure 3: AFCS basic sketch

Sensor selection and modeling

The states of the model description do not deliver direct information about the load pendulum sway. Thus, the pendulum motions, which are to be controlled, must be measured and provided as output variables. Different types of sensors are considered: For instance, an IMU that is mounted on the load can measure the body rates and transmit the data to the helicopter for further processing. Another approach is the installation of a sensing arm that follows the motions of the rod as an indicator for the load dynamic.

In general, sensors that do not require to transmit the information of the load dynamic from the load system to the helicopter system are advantageous, because then system complexity is kept to a minimum, which in turn leads to higher reliability. For this reason, a camera sensor featuring digital image processing for measuring the pendulum dynamic is chosen: A camera, which is mounted underneath the helicopter, tracks an optical marker (OM), which is placed on the load or at the slings, and generates visual information of the load position and velocity with reference to the helicopter body system (fig. 2). The load pendulum angles $\dot{\bar{\varphi}}_P$ and $\dot{\bar{\vartheta}}_P$ in the helicopter body system are then determined. These data are further processed using the helicopter attitude and body rates – measured by the onboard IMU – in order to derive the controller variables $\dot{\varphi}_P$ and $\dot{\vartheta}_P$, which describe the load pendulum motion in the geodetic system.

This kind of sensor was developed by iMAR GmbH [5] and means the basis for the simulation setup. The digital image processing provides short time delays as well as sample rates, which are sufficiently high concerning the rather slow load pendulum dynamic. Figure 2 shows the mounting position of the camera; its field of view covers an opening angle of 60°, which can be extended to 180° at the expense of process time.

Besides the derivation of the system pendulum angles and rates, the digital image processing includes KÁLMÁN-filtering for the simulated prediction of the position of the optical marker. The load dynamics is calculated by means of a simplified analytical pendulum model. This information is needed, in case the external load is not located within the camera field of view, due to large pendulum deflection angles, for instance.

State space model

The equations of motion in (58), (59) and (61) describe the overall system *helicopter and sling load*, and are used in the numerical simulation in their full nonlinear formulation. For analyses of the flight dynamics – for instance, stability and controllability – the system of equations must be simplified. For this, the state variables are bound to a working point, in order to enable a linearization: The theory of linear systems considers stationary flight conditions at an operating point $\boldsymbol{x}_0$. For the analysis and synthesis of linear systems, a multiplicity of tools – time-domain based as well as complex-variable-domain based – is available.

The linearization of the overall system leads to the state space model:

$$(1) \quad \dot{\boldsymbol{x}} = \boldsymbol{A}\boldsymbol{x} + \boldsymbol{B}\boldsymbol{u} \quad \text{(state equation)}, \ \boldsymbol{x}(0) = \boldsymbol{x}_0$$

$$(2) \quad \boldsymbol{y} = \boldsymbol{C}\boldsymbol{x} + \boldsymbol{D}\boldsymbol{u} \quad \text{(output equation)}$$

The state vector is given with

$$(3) \quad \boldsymbol{x} = [\boldsymbol{x}_H, \boldsymbol{x}_R, \boldsymbol{x}_L]^T$$

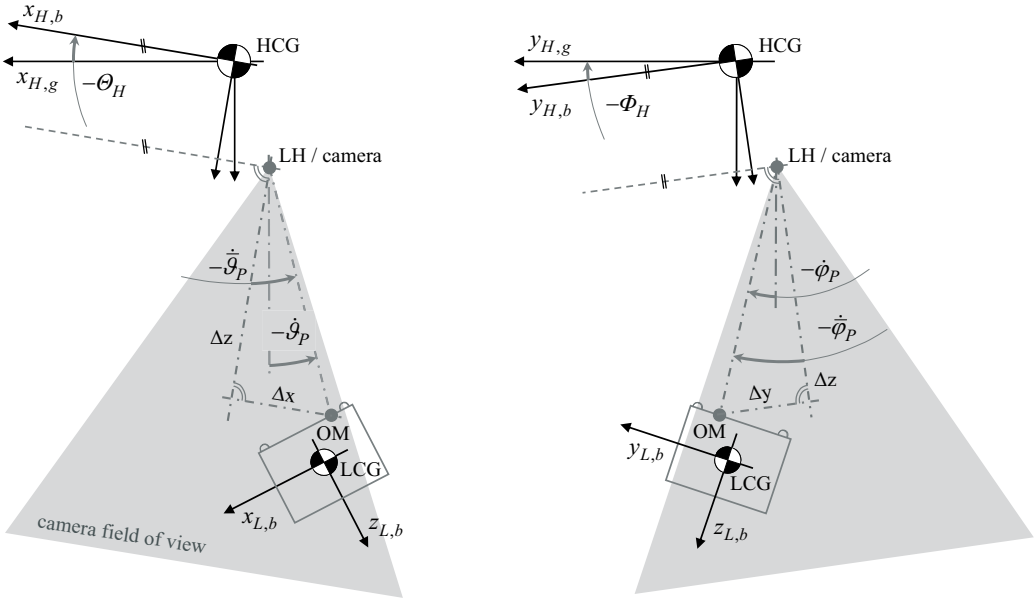

Figure 2: Sensor installation

including the helicopter/load states ($\Lambda = H, L$)

$$\boldsymbol{x}_\Lambda = (u, v, w, p, q, r, \Phi, \Theta)_\Lambda \quad (4)$$

and the states of the rod

$$\boldsymbol{x}_R = \left(\varphi, \dot{\vartheta}\right)_R \quad (5)$$

and the control vector

$$\boldsymbol{u} = [\delta c, \delta b, \delta a, \delta p]^T \quad (6)$$

as well as the output vector

$$\boldsymbol{y} = \left[\; (u, v, w, p, q, r, \Phi, \Theta)_H \, , \left(\varphi, \dot{\varphi}, \vartheta, \dot{\vartheta}\right)_P \; \right]^T \quad (7)$$

The system state matrix consists of the main matrices of the partial systems and the respective coupling matrices

$$\boldsymbol{A} = \begin{bmatrix} \boldsymbol{A}_H & \boldsymbol{A}_{R\to H} & \boldsymbol{A}_{L\to H} \\ \boldsymbol{A}_{H\to R} & \boldsymbol{A}_R & \boldsymbol{A}_{L\to R} \\ \boldsymbol{A}_{H\to L} & \boldsymbol{A}_{R\to L} & \boldsymbol{A}_L \end{bmatrix} \quad (8)$$

where the submatrix $\boldsymbol{A}_H$ contains the classical helicopter derivatives. The control matrix results in

$$\boldsymbol{B} = \begin{bmatrix} \boldsymbol{B}_H \\ \boldsymbol{B}_R \\ \boldsymbol{0} \end{bmatrix} \quad (9)$$

with $\boldsymbol{B}_L = \boldsymbol{0}$. The observer matrix is given with

$$\boldsymbol{C} = \begin{bmatrix} \boldsymbol{C}_H & \boldsymbol{0}_{(8x2)} & \boldsymbol{0}_{(8x8)} \\ \boldsymbol{C}_{H\to P} & \boldsymbol{C}_{R\to P} & \boldsymbol{C}_{L\to P} \end{bmatrix} \quad (10)$$

For the given system the feedthrough matrix is a zero matrix:

$$\boldsymbol{D} = \boldsymbol{0}_{(12x4)} \quad (11)$$

3 Analysis of the System Flight Dynamics

The flight dynamics describes the character of the motions of the overall linear system; one important result is the stability analysis. Applied for a cubical load without aerodynamics, figures 4 and 5 show the eigenmodes of the helicopter and the load at 60 kts forward level flight. The considered weight of the cube is 3000 kg and the length of the single sling is 7 m.

The incorporated degrees of freedom within the eigenmodes were analyzed using the corresponding eigenvectors. A characterization is given in table 1. The eigenmodes *I, II, V, VI, VII, VIII* mainly describe the helicopter dynamic, slightly coupled with the load dynamic. As a coupled motion of the systems *helicopter-rod-load*, the pendulum oscillation is described by the eigenmodes *III* (lateral) and *IV* (longitudinal). A vertical oscillation of high frequency is given by *IX*: The mode couples the vertical axes of the helicopter and the load by the flexible sling. The incorporation of the dynamics of the two degrees of freedom of the rod are described in *X* and *XI*. They are both of high frequencies, because of high constraining forces acting at the rather light rod of 50 kg. Besides the pendulum motions, the single suspended cube executes pitch and roll, which finds its expression in the

Table 1: Characterization of eigenmodes

eigenmode	characteristic	eigenmode	characteristic
I	helicopter roll mode	VIII	coupled helicopter longitudinal motion
II	helicopter dutch-roll mode	IX	coupled vertical oscillation
III	coupled lateral pendulum motion	X	coupled DmL lateral oscillations
IV	coupled longitudinal pendulum motion	XI	coupled DmL longit. oscillations
V	helicopter lateral- and roll mode	XII	load pitch mode
VI	helicopter roll mode	XIII	load roll mode
VII	coupled helicopter vertical motion		

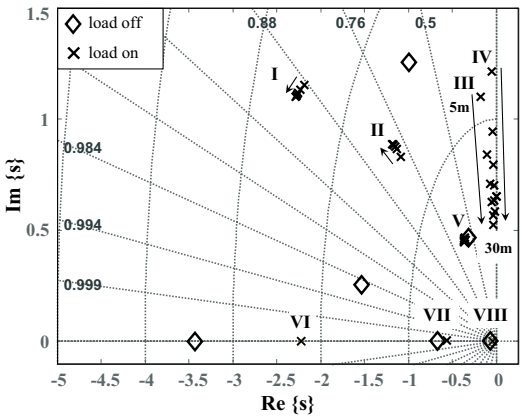

(a) close-up range

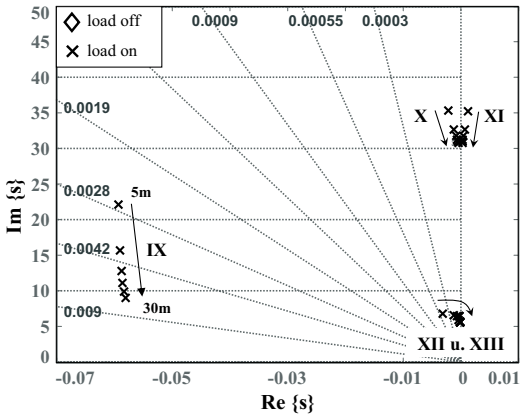

(b) far-field range

Figure 4: Pole-zero maps for a steady-state horizontal flight at $60\,kts$ with a $3000\,kg$ sling load, and a variation of sling length

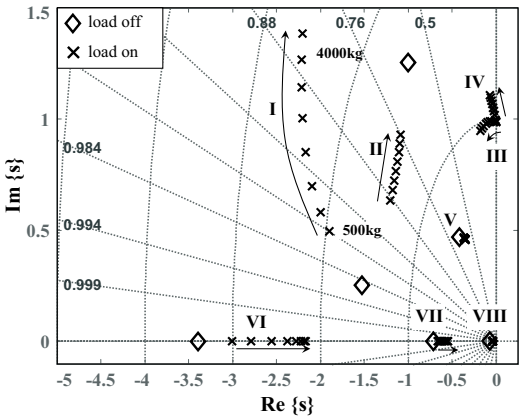

(a) close-up range

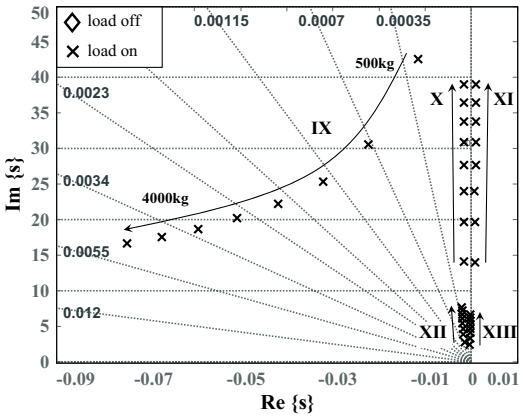

(b) far-field range

Figure 5: Pole-zero maps for a steady-state horizontal flight at $60\,kts$ with a $7\,m$ sling, and a variation of load weight

eigenmodes *XII* and *XIII*. Due to the lack of aerodynamic stabilization, the load's yaw motion has neutral stability, caused by the yaw hinge of the rod – it is located in the point of origin, and is not shown for clarity reasons.

Depending on system parameters like the cable length and the load mass, the eigenmodes of the overall system vary – particularly the pendulum motions in *III* and *IV*. The overall system shows a tendency to developing marginally stable pendulum motions (fig. 4 and 5). When increasing the sling length, the frequencies of the eigenmodes *III* and *IV* decrease, as well as of the vertical motion in *IX*, since the sling spring constant is a function of its length (fig. 4b). By increasing the load weight, the pendulum frequencies rise (fig. 5a). This effect can be explained by a simplified two-point dumb-bell model with the pendulum frequency given by (q.v. [6]):

$$\omega_P = \sqrt{\frac{g}{l_S} \cdot \left(1 + \frac{m_L}{m_H}\right)} \quad (12)$$

Since the helicopter roll rate in *I* and *II* is coupled with the load weight, the change in the pendulum frequency affects these eigenmodes, too – the damping declines with an increase in load weight. Furthermore, helicopter body-rates are controlled by the AFCS, which further amplifies the reciprocal effect of decreasing system damping as result of increasing system weight.

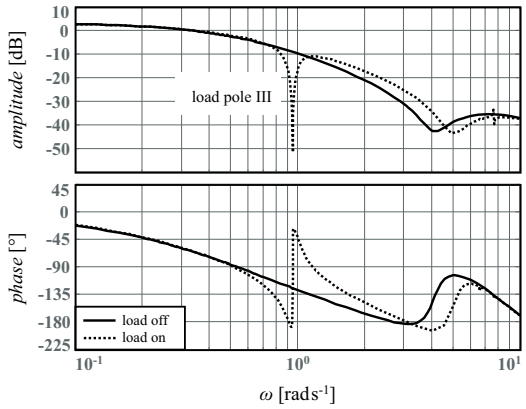

(a) $G_{\delta a\,\dot{y}_H}(s)$

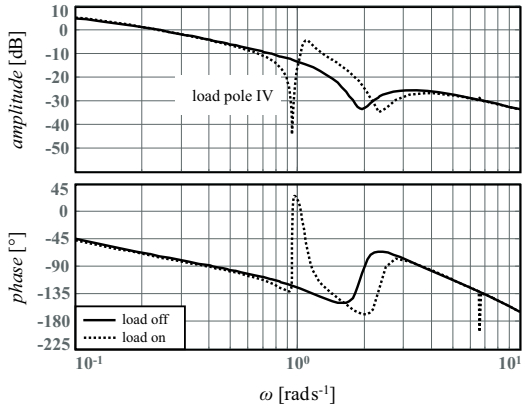

(b) $G_{\delta b\,\dot{x}_H}(s)$

Figure 6: Frequency responses of the translational helicopter velocities at $V = 0\,kts$, $m_L = 4000\,kg$, and $l_S = 7\,m$

4 Position Controllers

4.1 Problem Analysis

The positioning of helicopter sling loads is a twofold task. On the one hand, the load must be held on its position under the influence of disturbances. On the other hand, the load must be placed precisely from one position to another with minimal load sway.

For the development of positioning controllers, a reference flight case is considered featuring the key variables $V = 0\,kts$ defining hover state, $m_L = 4000\,kg$ as maximum load weight in addition to the helicopter weight, and $l_S = 7\,m$ for a short sling leading to quick pendulum motions.

Hoh et al. analyzed the dynamic impact of sling loads on the handling qualities of a CH-47D Chinook helicopter [7]. One essential output was that the controllability of the translational displacement of the helicopter is degraded due to the presence of a sling load. This effect intensifies with an increase in load weight. The dynamic influence of a sling load on the lateral and longitudinal helicopter speed above ground due to cyclic control inputs – expressed by the transfer functions $G_{\delta a\,\dot{y}_H}(s)$ and $G_{\delta b\,\dot{x}_H}(s)$ – of the CH-53D reference flight case is shown in figure 6.

The solid lines indicate the helicopter without the external load whereas the dotted lines illustrate the transfer behaviour of the translational displacement with the load attached. Considering the latter case, it can be seen that the poles of the pendulum oscillations – pole *III* for the lateral and pole *IV* for the longitudinal pendulum motion – considerably affect the dynamics of the translational helicopter displacement: The amplitude margins as well as the gain margins are lowered.

Hence, when positioning the helicopter in order to place the load, the load pendulum motions must be considered in the control strategy, too. Otherwise, the helicopter will be moved out of its target position constantly due to the coupling influence of the swinging load. Thus, the need for an integrated control of the translational displacement of the helicopter together with the pendulum dynamic is determined.

This integrated control task of positioning a load and damping its oscillation simultaneously is well known from the gantry-crane control. Significant contributions were made by Iordanou in [8] and [9], and by Corriga in [10], and by Wang and Surgenor in [11] and [12], for instance. They realized optimal

feedback control by using linear quadratic state regulation (LQR) in order to position the load time-optimal with minimal load sway. This approach was adapted for the helicopter sling load positioning task at hand. The goal is to position the helicopter, and simultaneously damp the load pendulum motions. Hence, by the time of arrival at the target position, the load's position is perpendicular and stable beneath the helicopter.

4.2 Controller selection aspects

The LQR-control is well suited for the interacting control of multi-variable systems. By means of a performance criterion, which is specially tailored to the objective of the control task, control parameters are determined, which deliver optimal results for the purpose of a weighting of the state and control variables. The controller is derived as solution of an optimization problem. For the correct application of LQR-control, all state variables must be measurable.

However, since the load pendulum motions are detected by means of a camera and digital image processing, the states of the load-body in $\boldsymbol{x}_L$ cannot be measured and thus, the full state vector cannot be determined. The consideration of a deterministic or stochastic observer may ease the problem. Another method of optimal control is given with the linear quadratic optimal output control: The weighted optimal control is accomplished by feedback of the position offset and the pendulum deflections. Compared to the observer design, this approach is advantageous because of a minor implementation complexity. The structure of the control loop is illustrated in figure 7. A turbulence model according to LUSARDI et al. in [13] is implemented and adapted to the CH-53 helicopter in order to test the achievable load-position accuracy under the influence of a turbulent atmosphere. Additional control inputs apply:

$$(13)\quad (\boldsymbol{u}_{turb})_H = [\delta c, \delta b, \delta a, \delta p]^T_{turb,H}$$

Furthermore, the turbulences affect the load aerodynamics, leading to additional inflow:

$$(14)\quad (\boldsymbol{x}_{turb})_L = [u, v, w]^T_{turb,L}$$

In case of a load displacement from a current position $\boldsymbol{P}_0$ to a desired target position $\boldsymbol{P}_{trgt}$, the helicopter velocity in $(u, v, w)_H$ and the covered distance $(\Delta x, \Delta y)^{\Psi_H=0}_{H,g}$ are determined by means of the integration of the measured body accelerations and the attitude of the helicopter in Φ_H and Θ_H. Here, $\Psi_H = 0$ denotes that the geodetic system is turned by the azimuth Ψ_H (fig. 8). The target position as well as the starting time t_0 for positioning could be commanded by the pilot, for instance. The control variables for positioning the helicopter are given with the position offset and its derivatives in equation (15) according figure 8.

$$(15)\quad \begin{pmatrix} \Delta x \\ \Delta y \end{pmatrix}^{\Psi_H=0}_{ctvr} = \underbrace{\begin{pmatrix} x \\ y \end{pmatrix}^{\Psi_H=0}_{trgt,H,g}}_{=\boldsymbol{P}_{trgt}} - \begin{pmatrix} x \\ y \end{pmatrix}^{\Psi_H=0}_{cur,H,g}$$

with

$$(16)\quad \begin{pmatrix} x \\ y \end{pmatrix}^{\Psi_H=0}_{trgt,H,g} = \begin{pmatrix} \Delta x \\ \Delta y \end{pmatrix}^{\Psi_H=0}_{cmd} + \underbrace{\begin{pmatrix} x \\ y \end{pmatrix}^{\Psi_H=0}_{H,0,g}}_{=\boldsymbol{P}_0=\boldsymbol{0}}$$

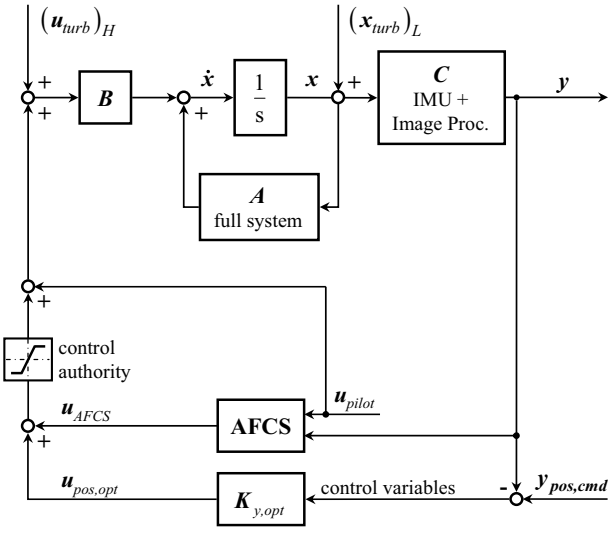

Figure 7: Output regulation

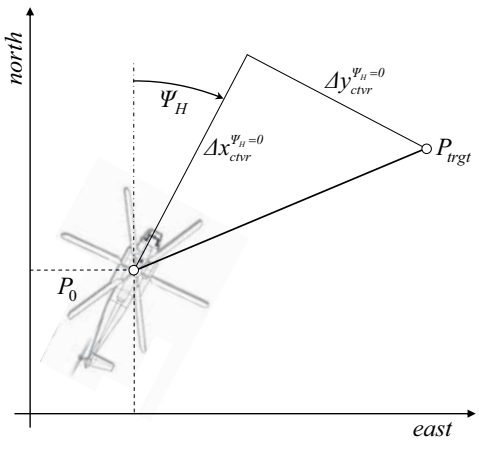

Figure 8: Position control signals

and

$$\left(\begin{array}{c} x \\ y \end{array} \right)_{cur,H,g}^{\Psi_H=0} = (TM)_{gb}^{\Psi_H=0} \cdot \int_{t_0}^{t} \left(\begin{array}{c} u \\ v \\ w \end{array} \right)_{H,b} dt + \underbrace{\left(\begin{array}{c} x \\ y \end{array} \right)_{0,H,g}^{\Psi_H=0}}_{=\boldsymbol{P}_0=\mathbf{0}} \tag{17}$$

The control variable of the position velocity is given with

$$\left(\begin{array}{c} \Delta\dot{x} \\ \Delta\dot{y} \end{array} \right)_{ctvr}^{\Psi_H=0} = \underbrace{\left(\begin{array}{c} \dot{x} \\ \dot{y} \end{array} \right)_{trgt,H,g}^{\Psi_H=0}}_{=\mathbf{0}} - \left(\begin{array}{c} \dot{x} \\ \dot{y} \end{array} \right)_{cur,H,g}^{\Psi_H=0} \tag{18}$$

and

$$\left(\begin{array}{c} \dot{x} \\ \dot{y} \end{array} \right)_{cur,H,g}^{\Psi_H=0} = (TM)_{gb}^{\Psi_H=0} \cdot \left(\int_{t_0}^{t} \left(\begin{array}{c} \dot{u} \\ \dot{v} \\ \dot{w} \end{array} \right)_{H,b} dt + \left(\begin{array}{c} u \\ v \\ w \end{array} \right)_{H,b}^{\Psi_H=0} \right) \tag{19}$$

considering

$$(TM)_{gb}^{\Psi_H=0} = \left(\begin{array}{ccc} \cos\Theta & \sin\Theta\sin\Phi & \sin\Theta\cos\Phi \\ 0 & \cos\Phi & -\sin\Phi \end{array} \right)_H \tag{20}$$

Besides the position offset of the helicopter and its derivation, the pendulum angles and rates are needed for feedback control:

$$\left(\begin{array}{c} \Delta\varphi \\ \Delta\vartheta \end{array} \right)_{P,H,b} = \underbrace{\left(\begin{array}{c} \varphi \\ \vartheta \end{array} \right)_{cmd,P}}_{=\mathbf{0}} - \left(\begin{array}{c} \varphi \\ \vartheta \end{array} \right)_{cur,P} \tag{21}$$

$$\left(\begin{array}{c} \Delta\dot{\varphi} \\ \Delta\dot{\vartheta} \end{array} \right)_{P,H,b} = \underbrace{\left(\begin{array}{c} \dot{\varphi} \\ \dot{\vartheta} \end{array} \right)_{cmd,P}}_{=\mathbf{0}} - \left(\begin{array}{c} \dot{\varphi} \\ \dot{\vartheta} \end{array} \right)_{cur,P} \tag{22}$$

Hence, the complete output vector for the linear quadratic optimal output control is given with:

$$\boldsymbol{y} = \left[(\Delta x, \Delta\dot{x}, \Delta y, \Delta\dot{y})_{H,g}^{\Psi_H=0}, \left(\Delta\varphi, \Delta\dot{\varphi}, \Delta\vartheta, \Delta\dot{\vartheta} \right)_{P,H,b} \right]^T \tag{23}$$

4.3 Linear Quadratic Output Regulation

The condition for optimality of the output regulation corresponds to the demand that a pre-defined performance index J must be minimized during the changeover of the system from the initial state $\boldsymbol{x}_0$ to the final state $\boldsymbol{x}_e$ in the time intervall $t \in [0, t_e]$. Generally, the performance criterion is quadratic, weighting system states as well as control deflections. Hence, the optimal controller is not derived against the background of fulfilling demands on the performance of the dynamic of the control loop. Instead, it is determined by the evaluation of the progress of the state and control variables within a considered time period. For the linear and time-invariant system of the equations (1) and (2), and the output feedback

$$\boldsymbol{u}(t) = -\boldsymbol{K}_y\, \boldsymbol{y}(t) \tag{24}$$

the time-variant performance index is formed in dependence on [14]:

$$\begin{aligned} J(\boldsymbol{x}_0, \boldsymbol{u}(t)) &= \boldsymbol{y}'(t_e)\boldsymbol{S}\boldsymbol{y}(t_e) \\ &\quad + \int_0^{t_e} \boldsymbol{x}'(t)\boldsymbol{C}'\boldsymbol{Q}_y\boldsymbol{C}\boldsymbol{x}(t) \\ &\quad + \boldsymbol{u}'(t)\boldsymbol{R}\boldsymbol{u}'(t)\; dt \end{aligned} \tag{25}$$

The achieved outputs in $\boldsymbol{y}(t_e)$ – as deviations from the desired output $\boldsymbol{y} = \mathbf{0}$ – are evaluated by means of $\boldsymbol{S}$. High control deflections are unfavorable and are therefore penalized by $\boldsymbol{R}$. The progress in the output variables $\boldsymbol{y}$ is rated by the evaluation matrix $\boldsymbol{Q}_y$. The matrices $\boldsymbol{S}$, $\boldsymbol{R}$ and $\boldsymbol{Q}_y$ are symmetric and positive definite. In the following, the formulas of the linear quadratic output regulation are explained for the sake of completeness.

The aim in LQ is a stationary feedback gain matrix $\boldsymbol{K}_y$ by means of the minimization of the performance index J of equation (25). The feedback control must be independent on the initial state $\boldsymbol{x}_0$ and time-invariant. By neutralizing the time limitation, equation (25) changes to the infinite time quadratic performance criterion. Hence, with

$$\boldsymbol{y}(t \to \infty) = \mathbf{0} \tag{26}$$

the output evaluation by $\boldsymbol{S}$ can be omitted. In order to use the performance criterion to find an optimal feedback gain matrix that is suitable for different flight states the dependence on $\boldsymbol{x}_0$ must be eliminated. For this, the performance obtained for a linear independent set of initial states is averaged. This corresponds to the assumption of the initial states in $\boldsymbol{x}_0$ being a random variable uniformly distributed on the surface of the n-dimensional unit sphere. Considering the expected value E of the n-initial states

$$E\{\boldsymbol{x}_0\, \boldsymbol{x}_0'\} = \frac{1}{n}\boldsymbol{U} \tag{27}$$

the optimization problem is given with:

$$\min_{\boldsymbol{K}_y} E\{J\} = \min_{\boldsymbol{K}_y} E\Big\{ \int_0^\infty \boldsymbol{x}'(t)\boldsymbol{C}'\boldsymbol{Q}_y\boldsymbol{C}\boldsymbol{x}(t) + \boldsymbol{u}'(t)\boldsymbol{R}\,\boldsymbol{u}'(t)\; dt \Big\} \tag{28}$$

The solution of (28) as a result of the minimization of the expected value E by the adaptation of $\boldsymbol{K}_y$ leads to the optimal time-invariant feedback control $\boldsymbol{K}_{y,opt}$, which is effective independent of the initial states.

The overall system from (1) is rewritten to

$$\dot{\boldsymbol{x}}(t) = \underbrace{\boldsymbol{A} - \boldsymbol{B}\boldsymbol{K}_y\boldsymbol{C}}_{\overline{\boldsymbol{A}}}\,\boldsymbol{x}(t)\;,\;\; \boldsymbol{x}(0) = \boldsymbol{x}_0 \tag{29}$$

In addition, $\boldsymbol{x}(t)$ is given with

$$\boldsymbol{x}\,(t) = \boldsymbol{x}_0\, e^{\overline{\boldsymbol{A}}\,t} \tag{30}$$

Substituting (30) into the performance criterion leads to

$$J = \int_0^\infty \boldsymbol{x}_0' e^{\overline{\boldsymbol{A}}'t}\,\overline{\boldsymbol{Q}}\,e^{\overline{\boldsymbol{A}}\,t}\boldsymbol{x}_0'\; dt = \boldsymbol{x}_0'\,\boldsymbol{P}\,\boldsymbol{x}_0 \tag{31}$$

with

$$\boldsymbol{P} = \int_0^\infty e^{\overline{\boldsymbol{A}}'t}\,\overline{\boldsymbol{Q}}\,e^{\overline{\boldsymbol{A}}\,t}\; dt \tag{32}$$

and

$$\overline{\boldsymbol{Q}} = \left(\boldsymbol{C}'\boldsymbol{Q}_y\boldsymbol{C} + \boldsymbol{C}'\boldsymbol{K}_y'\boldsymbol{R}\boldsymbol{K}_y\boldsymbol{C}\right) \tag{33}$$

By means of partial integration the matrix $\boldsymbol{P}$ is transformed to the linear Riccati-equation:

$$\overline{\boldsymbol{A}'}\,\boldsymbol{P} + \boldsymbol{P}\overline{\boldsymbol{A}} = -\overline{\boldsymbol{Q}} \tag{34}$$

For the symmetric matrix $\boldsymbol{P}$ – as the solution of the Riccati-equation – it applies:

$$\begin{aligned} \min_{\boldsymbol{K}_y} E\{J\} &= \min_{\boldsymbol{K}_y} E\{\boldsymbol{x}_0'\,\boldsymbol{P}\,\boldsymbol{x}_0\} \\ &= \min_{\boldsymbol{K}_y} E\{trace\,(\boldsymbol{P}\,\boldsymbol{x}_0\,\boldsymbol{x}_0')\} \end{aligned} \tag{35}$$

According to (28) and the initial state $\boldsymbol{x}_0$ – which is located on the unit sphere of (27) – and according to the fact that the expected value of the trace of $\boldsymbol{P}$ equals the trace of $\boldsymbol{P}$ itself, hence, the optimization of the expected value leads to the final form of the optimization problem:

$$\min_{\boldsymbol{K}_y} E\{J\} = \min_{\boldsymbol{K}_y} \frac{1}{n}\,trace\,(\boldsymbol{P}) = \min_{\boldsymbol{K}_y} \frac{1}{n}\,\overline{J} \tag{36}$$

The minimum of the function $\overline{J}$ is derived by means of nonlinear optimization: A steepest descent algorithm with Armijo-stepsizes was chosen.

For the search of the minimum of the modified criterion $\overline{J}$, the gradient of the trace of $\boldsymbol{P}$ is determined with respect to the elements in $\boldsymbol{K}_y$. The gradient features the characteristic to always point towards the direction of the steepest descent. The approximation of the extreme values follows this direction, and it is therefore inevitably arriving at a local minimum. The gradient matrix is given by the following equation according to [14], [15], [16]

$$\frac{\partial\overline{J}}{\partial\boldsymbol{K}_y} = 2\left(\boldsymbol{R}\,\boldsymbol{K}_y\,\boldsymbol{C} - \boldsymbol{B}'\,\boldsymbol{P}\right)\,\boldsymbol{L}\,\boldsymbol{C}' \tag{37}$$

and $\boldsymbol{P}$ as the solution of the Riccati-equation in (34) with

$$\begin{aligned} &(\boldsymbol{A} - \boldsymbol{B}\boldsymbol{K}_y\boldsymbol{C})\,\boldsymbol{P} + \boldsymbol{P}\,(\boldsymbol{A} - \boldsymbol{B}\boldsymbol{K}_y\boldsymbol{C})' \\ &\quad + \left(\boldsymbol{C}'\boldsymbol{Q}_y\boldsymbol{C} + \boldsymbol{C}'\boldsymbol{K}_y\boldsymbol{R}\boldsymbol{K}_y\boldsymbol{C}\right) = \boldsymbol{0} \end{aligned} \tag{38}$$

and $\boldsymbol{L}$ as the solution of the Ljapunow-equation:

$$(\boldsymbol{A} - \boldsymbol{B}\boldsymbol{K}_y\boldsymbol{C})\,\boldsymbol{L} + \boldsymbol{L}\,(\boldsymbol{A} - \boldsymbol{B}\boldsymbol{K}_y\boldsymbol{C})' + \boldsymbol{U} = \boldsymbol{0} \tag{39}$$

The minimum is arrived when the norm of the gradient approaches the pre-defined break value ϵ:

$$\left\| \frac{\partial\overline{J}}{\partial\boldsymbol{K}_y} \right\| < \epsilon \tag{40}$$

For the search of the minimum of the performance criterion by the variation of the elements in $\boldsymbol{K}_y$, the value of $\overline{J}$ is calculated along the gradient. A starting point $\boldsymbol{K}_{y,0}$ of the approximation method for the function $\overline{J} \in \mathbb{R}^n$ must be determined for that the closed loop is stable. This first feedback gain matrix can either be derived by an iterative *trial-and-error* approach or by some formalized approach (e.g. [17]). The optimal solution is then approximated within i iterative steps starting from the initial feedback gain matrix. For the approximation a stepsize a is introduced, which is regulated by common techniques of unidimensional search: For the paper at hand, the Armijo condition was chosen. According to this procedure, the step size is controlled and adapted by the inequation (41). Hence, any overshooting beyond the minimum as a result of large step sizes is avoided as well as the conduction of too many steps of iteration due to very small step sizes. The performance index of the potentially more optimal controller $\boldsymbol{K}_{y,i+1}$ is compared to the current controller $\boldsymbol{K}_{y,i}$:

$$\overline{J}\left(\boldsymbol{K}_{y,i} - a_i\frac{\partial\overline{J}}{\partial\boldsymbol{K}_y}\right) - \overline{J}\,(\boldsymbol{K}_{y,i}) < \frac{a_i}{2}\left\langle \frac{\partial\overline{J}}{\partial\boldsymbol{K}_{y,i}}, \frac{-\partial\overline{J}}{\partial\boldsymbol{K}_{y,i}} \right\rangle \tag{41}$$

If the inequation (41) is satisfied, a new and more optimal controller is found:

$$\boldsymbol{K}_{y,i+1} = \boldsymbol{K}_{y,i} - a_i \cdot \frac{\partial\overline{J}}{\partial\boldsymbol{K}_y} \tag{42}$$

Consequently, the step size is increased for the next step of iteration:

$$(43)\quad a_{i+1} \;=\; \zeta \cdot a_i \qquad ,\zeta \geq 1\ .$$

If (41) is not satisfied, the step size a must be too large, leading to

$$(44)\quad \boldsymbol{K}_{y,i+1} \;=\; \boldsymbol{K}_{y,i}$$

and the lowering of a according to:

$$(45)\quad a_{i+1} \;=\; \xi \cdot a_i \qquad ,\xi < 1\ .$$

The step size is decreased until (41) is satisfied and a new controller is found. By means of the feedback gain $\boldsymbol{K}_{y,i+1}$ the RICCATI-equation in (38), and the LJAPUNOW-equation in (39), and the gradient according to (37) are determined. In a next step, the break condition in (40) is evaluated by its arrival the optimal controller is found:

$$(46)\quad \boldsymbol{K}_{y,opt} \;=\; \boldsymbol{K}_{y,i+1}$$

The process chain of the derivation of the optimal output control is once again illustrated in figure 9.

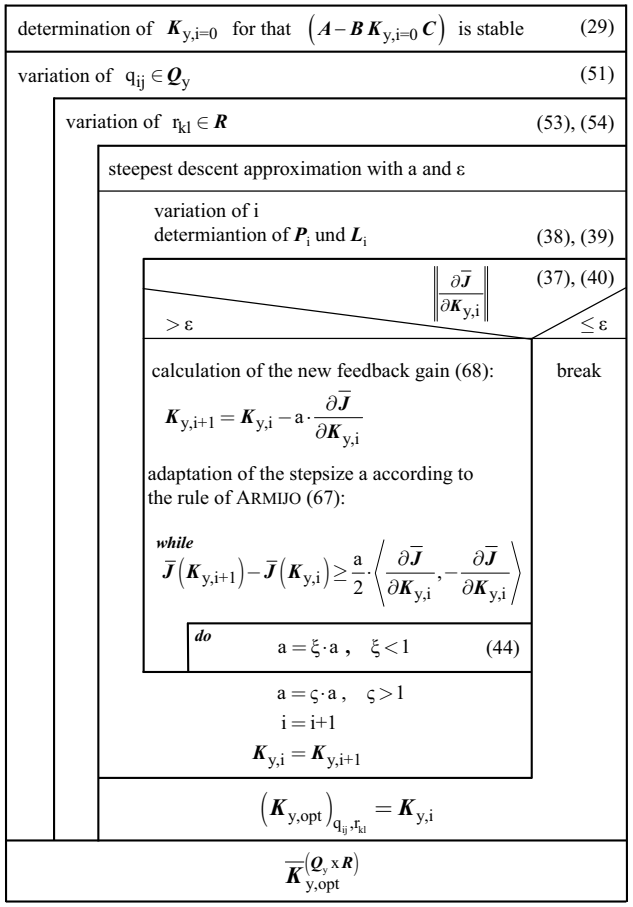

Figure 9: Algorithm for the determination of linear quadratic optimal output feedback regulation

An important task in the LQ optimal regulation is the agreement of the weighting matrices $\boldsymbol{Q}_y$ and $\boldsymbol{R}$. The ratio between the elements $q_{ij} \in \boldsymbol{Q}_y$ and $r_{kl} \in \boldsymbol{R}$ determines the control rate: Small values of r_{kl} lead to an increase in rate but require greater actuator amplitudes and vice versa.

The ratio among the elements q_{ij} determines, how fast the states are run to zero. Hence, the choice of $\boldsymbol{Q}_y$ and $\boldsymbol{R}$ is essential since they mean the basis for the evaluation of the progressions of the outputs and control variables.

A common approach to determine the weighting matrices is given with the *trial-and-error* method. The elements are varied without considering any interconnections nor dependencies between them. According to the number of system states, this procedure rapidly loses clearness and practicality due to a multliplicity of variations. In the paper at hand, the weighting elements are derived in general accordance to the method of WANG and SURGENOR [11]. The maximum deviations of the output variables q_{ij} as well as the maximum control deflections r_{kl} are defined as guideline values for subsequent parameter variations. The off diagonal elements of $\boldsymbol{Q}_y$ and $\boldsymbol{R}$ are assumed zero, and the q_{11} and q_{33} elements are set to one, which is the weighting of the helicopter position. This procedure seems adequate, since the weighting characteristic is determined by the ratio of the elements instead by their absolute values. Hence, there are four tunable parameters left: q_{55} and q_{77} for the weighting of the load angles, and r_{22} and r_{33} for the penalization of cyclic control deflections. The longitudinal and lateral motions are weighted separately so that the output weighting matrix is given with

$$(47)\quad \boldsymbol{Q}_y = \begin{pmatrix} 1 & 0 & 0 & 0 & 0 & 0 & 0 & 0 \\ & 0 & 0 & 0 & 0 & 0 & 0 & 0 \\ & & 1 & 0 & 0 & 0 & 0 & 0 \\ & & & 0 & 0 & 0 & 0 & 0 \\ & & & & \frac{(y_H)^2_{max}}{(\varphi_P)^2_{max}} & 0 & 0 & 0 \\ & \text{symm.} & & & & 0 & 0 & 0 \\ & & & & & & \frac{(x_H)^2_{max}}{(\vartheta_P)^2_{max}} & 0 \\ & & & & & & & 0 \end{pmatrix}$$

and the weighting matrix of the control inputs with

$$(48)\quad \boldsymbol{R} \;=\; \begin{pmatrix} 0 & 0 & 0 & 0 \\ & \frac{(x_H)^2_{max}}{(\delta b)^2_{max}} & 0 & 0 \\ & & \frac{(y_H)^2_{max}}{(\delta a)^2_{max}} & 0 \\ & \text{symm.} & & 0 \end{pmatrix}$$

For an assumed intervall of maximum position deviations of

$$(49)\quad (x_H, y_H)_{max} \;\in\; [5\,m\,,\,20\,m]$$

and an intervall of maximum pendulum angles of

$$(50)\quad (\varphi_P, \vartheta_P)_{max} \;\in\; [5^\circ\,,\,20^\circ]$$

the following variation range for q_{55} and q_{77} applies, relative to the remaining elements in $\boldsymbol{Q}_y$ and $\boldsymbol{R}$:

$$(51)\quad (q_{55}, q_{77}) \;\in\; [0.06\,,\,16]$$

The maximum allowed control deflections – the AFCS limits the cyclic control by ±10% – account for:

$$(52)\quad \begin{array}{rcl} (\delta b)_{max} & \approx & 3\,cm \\ (\delta a)_{max} & \approx & 2\,cm \end{array}$$

Thus, the variation ranges for r_{22} and r_{33} are:

$$(53)\quad r_{22} \;\in\; [2.6\,,\,41.5]$$

$$(54)\quad r_{33} \;\in\; [4.9\,,\,8.0]$$

The optimal feedback gains for various flight cases are determined within the intervals of $\boldsymbol{Q}_y$ and $\boldsymbol{R}$ by optimizing the performance criterion.

5 Performance Analysis

For the overall system illustrated in figure 14 at $V = 0\,kts$, $m_L = 4000\,kg$, and $l_S = 7\,m$ the linear quadratic optimal output regulation is adopted. In order to start the optimization algorithm the initial feedback gain matrix is set up, which stabilizes the system in equation (29):

$$(55)\quad \boldsymbol{K}_{y,0} = \begin{pmatrix} 0 & 0 & 0 & 0 & 0 & 0 & 0 & 0 \\ 1 & 2 & 0 & 0 & 0 & 0 & -0.1 & -0.1 \\ 0 & 0 & 1 & 2 & 0.1 & 0.1 & 0 & 0 \\ 0 & 0 & 0 & 0 & 0 & 0 & 0 & 0 \end{pmatrix}$$

The optimal feedback controllers $(\boldsymbol{K}_{y,opt})_{q_{ij},r_{kl}}$ – they have been determined in dependence on $\boldsymbol{Q}_y$ and $\boldsymbol{R}$ – are virtual-flight-tested on their ability to position the overall system in order to eventually define the optimal controller $\boldsymbol{K}_{y,opt}^{(\boldsymbol{Q}x\boldsymbol{R})}$. The meaning of the optimal positioning must be formulated by means of another performance criterion. For this, the criterion of equation (25) determining the system energy can be used. An alternative is given in the integration of the absolute error of the position offsets and the load pendulum deflections leading to:

$$(56)\quad J^* = \int_0^\infty \|\Delta x_H\| + \|\Delta y_H\| + \|\Delta \varphi_P\| + \|\Delta \vartheta_P\|\, dt$$

Analyses of both criteria showed that the positioning of the overall system leads to different results. Evaluating the integrated absolute errors yields more optimal results.

Figures 10 and 11 show the achievable minimal performance index J^* for the longitudinal and lateral positioning of the reference flight case due to the variation of the elements in $\boldsymbol{Q}_y$ and $\boldsymbol{R}$. The test case describes a positioning of the helicopter by $\Delta x = 20\,m$ in the longitudinal and by $\Delta y = 20\,m$ in the lateral direction, respectively: The position range was chosen arbitrary since it does not influence the resulting optimal weighting. The goal is to determine the weighting parameters q_{55}, q_{77}, r_{22}, and r_{33}, which lead to the optimal positioning of the overall system according to the performance criterion of equation (56).

The far field in figure 10a shows a decrease of J^* towards small values of q_{77} and r_{22}. For the determination of the performance index of the longitudinal positioning, the weighting parameters associated with the lateral positioning are set to one and thus, neutrally rated. Both optimization processes are therefore regarded as decoupled. In doing so, the processing time can be reduced. However, tests regarding a coupled variation of the weighting elements led to nearly congruent results. The minimal performance index is attained at $q_{77} = 0.35$ and $r_{22} = 1.6$ (q.v. fig. 10b). In case of the lateral positioning the weighting elements q_{77} and r_{22} are set to one, and the minimal performance index J^* is accomplished by the variation of

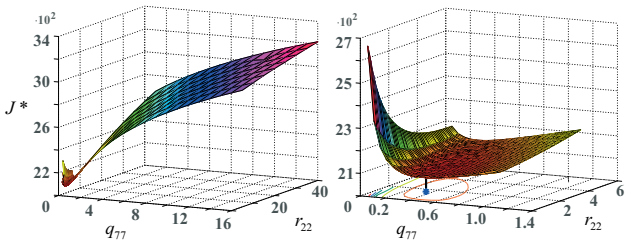

(a) far-field range (b) close-up range

Figure 10: Determination of the minimal performance index J^* of the longitudinal positioning by a variation of q_{77} and r_{22} at the reference flight case

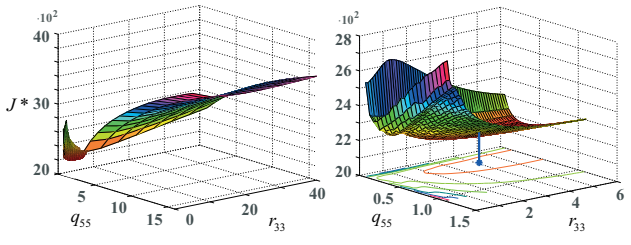

(a) far-field range (b) close-up range

Figure 11: Determination of the minimal performance index J^* of the lateral positioning by a variation of q_{55} and r_{33} at the reference flight case

q_{55} and r_{33}. Again, a decrease of the index develops and its minimum is achieved at $q_{55} = 0.3$ and $r_{33} = 4.1$ (q.v. fig. 11).

Eventually, the following optimal feedback control gain is determined for the reference flight case:

(57)

$$\boldsymbol{K}_{y,opt} = \begin{pmatrix} 0 & 0 & 0 & 0 & 0 & 0 & 0 & 0 \\ 0.32 & 1.44 & 0 & 0 & 0 & 0 & 0.07 & -0.10 \\ 0 & 0 & 0.27 & 1.09 & 0.05 & 0.13 & 0 & 0 \\ 0 & 0 & 0 & 0 & 0 & 0 & 0 & 0 \end{pmatrix}$$

The optimal positioning of the overall system is illustrated in figure 12. The helicopter is displaced by $20\,m$ longitudinally and laterally at the same time. The integrated load pendulum sway regulation is switched on in figure 12a and deactivated in 12b for comparison – hence, the control elements $\left(k_{(2,7)}, k_{(2,8)}, k_{(3,5)}, k_{(3,6)} \in \boldsymbol{K}_{y,opt}\right)$ are set to zero. The upper panes show the relative cyclic control inputs from the AFCS superposed by the automatic position control. The control limits of $\pm 10\%$ with reference to the trim control are not exceeded. It can be seen in figure 12a that the load sway is being damped during the system displacement towards the target position. By the time of the arrival at the final position the load pendulum motions are entirely damped and stabilized. If the load sway is not considered in the feedback control, the helicopter control will not be able to hold the position accurately due to a remaining load sway.

In a next step, the ability to hold the load position under the influence of turbulences is briefly analyzed. The disturbances affect the helicopter and the container; different turbulence intensities are considered

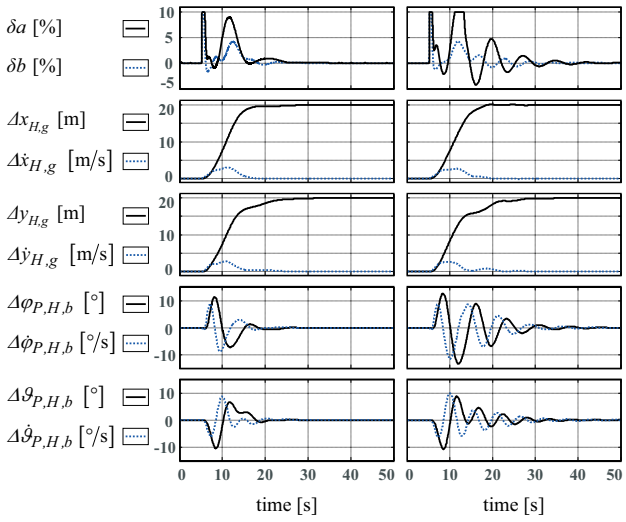

(a) integrated pendulum damping active (b) integrated pendulum damping inactive

Figure 12: Optimal positioning of the overall system by $\Delta x = \Delta y = 20\,m$ in the reference flight case

U_0		σ_w		intensity
$[ft/s]$	$[kts]$	$[ft/s]$	$[kts]$	
3	1.78	0.1	0.06	weak
10	5.92	0.6	0.36	normal
18	10.66	3.6	2.13	medium
28	16.58	7.1	4.20	strong

Table 2: Turbulence intensities

and listed in table 2, ranging from weak ($< 2\,kts$) to strong interferences ($> 15\,kts$) in dependence on [13].

The results of the position hold are illustrated in figure 13 for four different turbulence intensities over a period of 100 seconds. The different panes show the relative deviations of the helicopter position, the pendulum sway and the load position from the respective initial conditions. Furthermore, the longitudinal load deviation is plotted against its lateral displacement. In case of weak turbulences the load position can be held within a field of $20\,cm\ x\ 20\,cm$ edge length. This position accuracy decreases to $40\,cm\ x\ 40\,cm$ for normal turbulences down to $4\,m\ x\ 4\,m$ in case of strong turbulences, rather due to the helicopter dynamic than the pendulum oscillations.

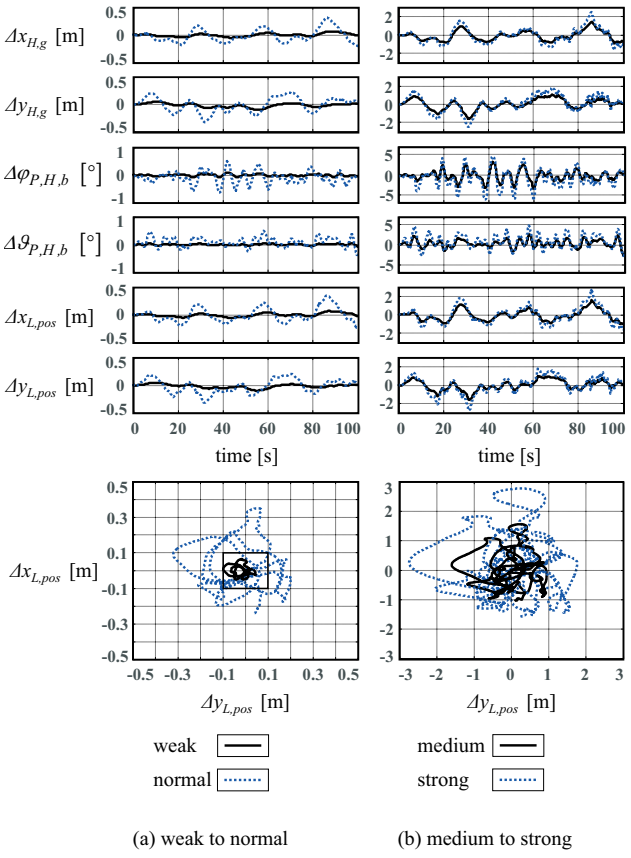

(a) weak to normal (b) medium to strong

Figure 13: Position hold accuracy of a $4t$-container in turbulent atmosphere

6 Conclusion and Outlook

Sling loads influence the helicopter dynamics. The handling qualities are degraded and the pilot workload is increased significantly due to the additional task to control the load. Analyses revealed that the translational dynamic of the helicopter is severely affected by the sling load. The need for pilot support is therefore evident: The paper at hand focusses on the development of supplementary AFCS-modes, which generate control inputs that combine the automatic helicopter positioning with an integrated load sway control.

On the basis of a comprehensive system simulation featuring trim calculation, linearization and virtual flight testing, position controllers are developed by means of an automatic optimization algorithm using linear quadratic optimal output regulation. Analyses show that the sling load can be positioned optimal in terms of the minimization of the time until the target position is reached and of the load sway. The LQ-controllers are effective within the operating range of the AFCS-actuators regarding the limited rate and saturation.

In a next step, the controller algorithm and the digital image processing system will be implemented into the DLR system simulator and the Flying Helicopter Simulator (FHS) in order to analyze the controller effectiveness for different helicopter types and system configurations, and to evaluate pilot acceptance.

Appendix

Rigid-body dynamics

In a first step, the helicopter and load are described separately as two independent six degree-of-freedom rigid bodies. The general equations of the nonlinear translational and rotatory motions are given by (58) and (59).

The index $\Lambda = (H, L)$ enunciates the compatibility of the equations for the helicopter and the load, respectively. For the validity of the rigid body expression, following conditions apply:

- the earth is considered as initial frame
- the helicopter and the load are considered as rigid bodies
- the helicopter and the load are symmetric relating to the xz-plane, leading to $I_{xy} = I_{yz} = 0$
- external forces are concentrated in resultant forces acting in the respective center of gravity

The rod is considered as additional body with two degrees of freedom; its dynamics is determined by angular-moment-theory in equation (61). Therefore, the dynamics of the overall system is described by the states

$$\begin{aligned} \boldsymbol{x}_H &= (u, v, w, p, q, r, \Phi, \Theta)_H \\ \boldsymbol{x}_L &= (u, v, w, p, q, r, \Phi, \Theta)_L \\ \boldsymbol{x}_R &= \left(\dot{\varphi}, \dot{\vartheta}\right)_R \end{aligned}$$

The general nonlinear equation of the translational motion is given by:

$$\left(\frac{d\boldsymbol{V}}{dt}\right)_{\Lambda,b} = \frac{1}{m_\Lambda} \cdot \sum \boldsymbol{F}_{\Lambda,b} - \boldsymbol{\omega}_{\Lambda,b} \times \boldsymbol{V}_{\Lambda,b} \tag{58}$$

and of the rotation by:

$$\begin{aligned} \left(\frac{d\boldsymbol{\omega}}{dt}\right)_{\Lambda,b} = \boldsymbol{I}_{\Lambda,b}^{-1} \cdot \Bigg[&\sum \boldsymbol{M}_{\Lambda,b}^{CG} \\ &- \boldsymbol{\omega}_{\Lambda,b} \times \left(\boldsymbol{I}_{\Lambda,b}^{-1} \cdot \boldsymbol{\omega}_{\Lambda,b}\right) \Bigg] \end{aligned} \tag{59}$$

applying for the helicopter and the load ($\Lambda = (H, L)$).

The rod is considered as additional body with two degrees of freedom:

$$\left(\frac{d\boldsymbol{\omega}}{dt}\right)_{R,b} = \left(\ddot{\varphi}, \ddot{\vartheta}\right)_R^T \tag{60}$$

The analytical modeling is based on angular-moment-theory for systems, whose reference point is neither its center of gravity nor its fixed-point:

$$\begin{aligned} \left(\frac{d\boldsymbol{\omega}}{dt}\right)_{R,b} = \left(\boldsymbol{I}_{R,b}^{LH}\right)^{-1} \cdot \Bigg[&\sum \boldsymbol{M}_{R,b}^{LH} \\ &- m_R \cdot \left(\boldsymbol{r}_{LH\to R} \times \boldsymbol{a}_{LH,g}^{abs}\right) \Bigg] \end{aligned} \tag{61}$$

The sum of the resulting moments with respect to the load hook is derived by

$$\begin{aligned} \sum \boldsymbol{M}_{R,b}^{LH} = &- \frac{l_R\, m_R\, g}{2} \cdot \begin{bmatrix} \sin\varphi\, \cos\vartheta \\ \cos\varphi\, \sin\vartheta \\ \cos\varphi\, \cos\vartheta \end{bmatrix}_R \\ &+ \begin{bmatrix} 0 \\ 0 \\ l_R \end{bmatrix} \times \boldsymbol{F}_R^{sling} \end{aligned} \tag{62}$$

The absolute acceleration of the helicopter load hook in the geodetic system is obtained by

$$\boldsymbol{a}_{LH,g}^{abs} = \boldsymbol{T}\boldsymbol{M}_{gb}^{H} \cdot \boldsymbol{a}_{LH,b}^{abs} \tag{63}$$

and the absolute acceleration of the load hook in helicopter body-axes:

$$\begin{aligned} \boldsymbol{a}_{LH,b}^{abs} = \boldsymbol{a}_{H,b}^{abs} &+ \underbrace{\dot{\boldsymbol{\omega}}_{H,b} \times \boldsymbol{r}_{HCG\to LH}}_{\text{tangential acc.}} \\ &+ \underbrace{\boldsymbol{\omega}_{H,b} \times \left(\boldsymbol{\omega}_{H,b} \times \boldsymbol{r}_{HCG\to LH}\right)}_{\text{centripetal acc.}} \\ &+ \underbrace{2 \cdot \boldsymbol{\omega}_{H,b} \times \boldsymbol{v}_{LH,b}^{rel}}_{\text{coriolis acc.}} + \boldsymbol{a}_{LH,b}^{rel} \end{aligned} \tag{64}$$

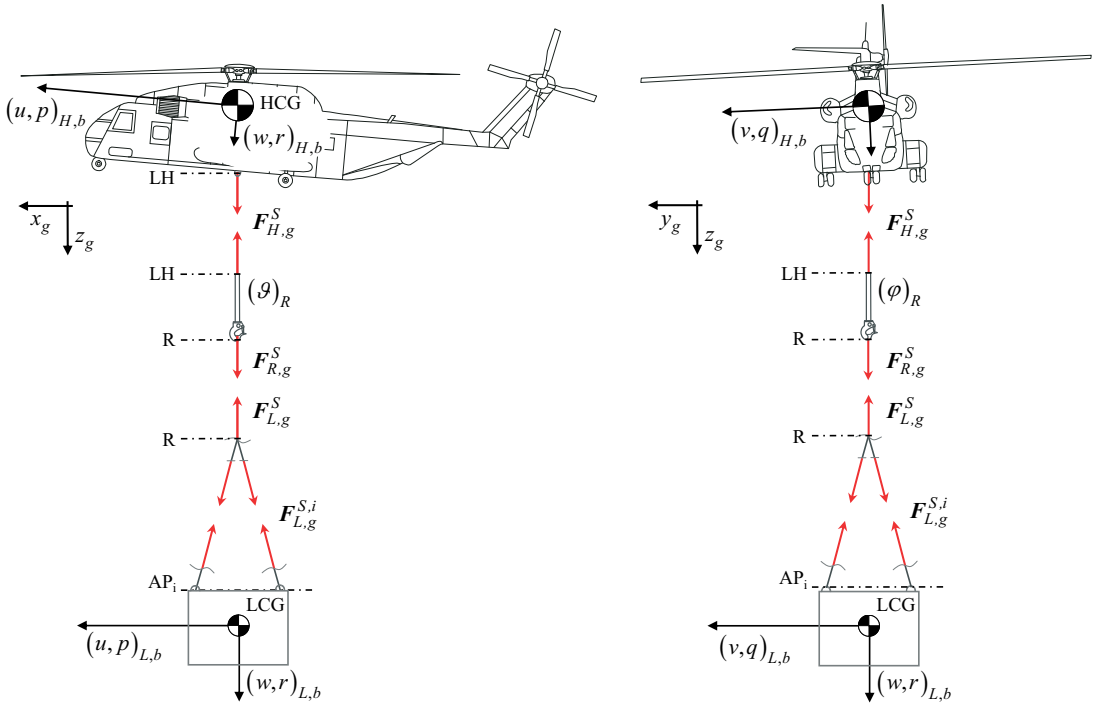

Figure 14: Overall system *helicopter, rod and sling load*

The distance between the helicopter center of gravity and the load hook remains constant. Hence, the relative acceleration $\boldsymbol{a}^{rel}_{LH,b}$ as well as the coriolis acceleration, both become zero.

The external forces and moments in the equations (58), (59), and (61) result from aerodynamics and the sling forces.

Aerodynamics

The container load features an edge length of $2.4\,m$. Its aerodynamic coefficients have been derived in wind tunnel tests. The polars of the static aerodynamic coefficients – which lead to a tangential, and two normal forces, and a moment – were identified in [4]. The resulting aerodynamic forces are derived by

$$\boldsymbol{F}^{A}_{L,b} = q_C \cdot \begin{pmatrix} C_X(\alpha_{xz})\,V^2_{xz} + C_X(\beta)\,V^2_{xy} \\ C_Y(\beta)\,V^2_{xy} + C_Y(\alpha_{yz})\,V^2_{yz} \\ C_Z(\alpha_{xz})\,V^2_{xz} + C_Z(\alpha_{yz})\,V^2_{yz} \end{pmatrix} \tag{65}$$

considering

$$q_C = \frac{\rho}{2} \cdot h_C \cdot w_C \tag{66}$$

$$\alpha_{xz} = \arctan\left(w/u\right) \tag{67}$$

$$\alpha_{yz} = \arctan\left(w/v\right) \tag{68}$$

$$V^2_{xz} = u^2 + w^2 \tag{69}$$

$$V^2_{xy} = u^2 + v^2 \tag{70}$$

$$V^2_{yz} = v^2 + w^2 \tag{71}$$

$$\beta = \arcsin \frac{v}{\sqrt{(u^2 + v^2 + w^2)}} \tag{72}$$

Due to the symmetry of the container, $C_Y = C_Z$ applies for the aerodynamic polar.

The polar of the aerodynamic moment coefficient C_M against the angle of attack indicates that for small angles $i = 0° = 90°$ and for $i \approx 15°$, the moment becomes zero [4]. For angles between 0° and 15°, the reaction moment is positive and hence stable; for all other angles, the moment is instable causing the container to spin around its yaw axis.

The aerodynamic moments depend on the cross section surface and the container length. They are given with

$$\boldsymbol{M}^{A}_{L,b} = q_C \cdot l_C \cdot \begin{pmatrix} C_M(\alpha_{yz})\,V^2_{yz} \\ C_M(\alpha_{xz})\,V^2_{xz} \\ C_M(\beta)\,V^2_{xy} \end{pmatrix} \tag{73}$$

The moments of inertia of the container used in equation (59) are calculated with

$$I_{L,xx} = \frac{m_L}{12}\left(h^2_C + w^2_C\right) \tag{74}$$

$$I_{L,yy} = \frac{m_L}{12}\left(l^2_C + h^2_C\right) \tag{75}$$

$$I_{L,zz} = \frac{m_L}{12}\left(l^2_C + w^2_C\right) \tag{76}$$

Constraining forces

The resultant vector of the sling forces in the respective body system ($\Lambda = H, R, L$) is given by the transformation of the vectors of the geodetic sling forces

$$(77) \quad \boldsymbol{F}^{S}_{\Lambda,b} = \boldsymbol{TM}^{\Lambda}_{bg} \cdot \sum_{i} \boldsymbol{F}^{S,i}_{\Lambda,g}$$

derived by the vectorial description of the sling force

$$(78) \quad \boldsymbol{F}^{S,i}_{\Lambda,g} = \left|\boldsymbol{F}^{S,i}\right| \cdot \begin{pmatrix} \sin\vartheta \cdot \cos\varphi \\ \cos\vartheta \cdot \sin\varphi \\ \cos\vartheta \cdot \cos\varphi \end{pmatrix}^{S,i}_{g}$$

which is determined for each sling due to its elongation and elongation rate:

$$(79) \quad \left|\boldsymbol{F}^{S,i}\right| = c_{S,i}\,\Delta l_{S,i} + d_{S,i}\,\dot{l}_{S,i}$$

The attitude of each sling is given by (q.v. fig.14):

$$(80) \quad \varphi^{S,i}_{g} = -\arctan\left(\frac{y_{AP} - y_R}{z_{AP} - z_R}\right)^{S,i}_{g}$$

$$(81) \quad \vartheta^{S,i}_{g} = -\arctan\left(\frac{x_{AP} - x_R}{z_{AP} - z_R}\right)^{S,i}_{g}$$

The moment vectors due to the sling forces in the helicopter and load body system are given by

$$(82) \quad \boldsymbol{M}^{S}_{H,b} = \left[\begin{bmatrix} x \\ y \\ z \end{bmatrix}^{LH}_{H,b} - \begin{bmatrix} x \\ y \\ z \end{bmatrix}^{HCG}_{H,b} \right] \times \boldsymbol{F}^{S}_{H,b}$$

and

$$(83) \quad \boldsymbol{M}^{S,i}_{L,b} = \left[\begin{bmatrix} x \\ y \\ z \end{bmatrix}^{AP,i}_{L,b} - \begin{bmatrix} x \\ y \\ z \end{bmatrix}^{LCG}_{L,b} \right] \times \boldsymbol{F}^{S,i}_{L,b}$$

References

[1] Brenner, H.: Flight Testing of Pioneer Bridges as Helicopter Slung Loads Using a CH-53G. In: *Proceedings of the 33rd European Rotorcraft Annual Forum*, 2007

[2] Brenner, H.: Simulation Model for Helicopter Cargo Handling Investigations. In: *Proceedings of the 7th ONERA-DLR Aerospace Symposium*, 2006

[3] Heffley, R.K. ; Jewell, W.F.: A Compilation and Analysis of Helicopter Handling Qualities Data - Volume One: Data Compilation / NASA Contractor Report 3144. 1979. – Technical Report

[4] Ronen, T.: *Dynamics of a Helicopter With a Sling Load*, Department of Aeronautics and Astronautics of Stanford University, Diss., August 1985

[5] *iMAR-GmbH, Gesellschaft für inertiale Mess-, Automatisierungs- und Regelsysteme.* `http://www.imar-navigation.de`

[6] Cicolani, L.S. ; McCoy, A.H. ; Tischler, M.B. ; Tucker, G.E.: Flight Time Identification of a UH-60A Helicopter and Slung Load, TM-1998-112231 / NASA Ames Research Center. 1998. – Technical Report

[7] Hoh, R.H. ; Heffley, R.K. ; D.G.Mitchell: Development of Handling Qualities Criteria for Rotorcraft with Externally Slung Loads / NASA, U.S. Army RDECOM. 2006. – Technical Report

[8] Iordanou, H.N. ; Surgenor, B.W.: Experimental Evaluation of the Robustness of Discrete Sliding Mode Control versus Linear Quadratic Control. In: *IEEE Transactions on Control Systems Technology* 5 (1997), S. 254–260

[9] Iordanou, H.N.: *Continuous Versus Discrete Sliding Mode Control as Applied to a Pneumatic Positioning System*, Queen's University, Canada, Diss., 1998

[10] Corriga, G. ; Guiua, A. ; Usai, G.: An Implicit Gain-Scheduling Controller for Cranes. In: *IEEE Transactions on Control Systems Technology* 6, No.1 (1998), S. 15–20

[11] Wang, Z. ; Surgenor, B.: Performance Evaluation of the Optimal Control of a Gantry Crane. In: *Proceedings of ASME International Mechanical Engineering Congress*, 2003

[12] Wang, Z. ; Surgenor, B.: A Problem with the LQ Control of Overhead Cranes. In: *Journal of Dynamic Systems, Measurement and Control* 128 (2006), S. 436–440

[13] Lusardi, J. A.: *Control Equivalent Turbulence Input Model for the UH-60 Helicopter*, University of California, Diss., 2004

[14] Lunze, J.: *Regelungstechnik 2, Mehrgrößensysteme, Digitale Regelung.* 4. Auflage. Springer-Verlag, 2006

[15] Yan, W.Y. ; Teo, K.L.: A Gradient Flow Approach to Computing LQ Optimal Output Feedback Gains. In: *Optimal Control Applications and Methods* 15, No.1 (1994), S. 67–75

[16] Levine, W.S. ; Athans, M.: On the Determination of the Optimal Constant Output Feedback Gains for Linear Multivariable Systems. In: *IEEE Transactions on Automatic Control* AC-15, No.1 (1970), S. 44–48

[17] Shapiro, E.Y. ; Fredricks, D.A.: *Lecture Notes in Control and Information Sciences, paper: Application of Constrained Constant Optimal Output Feedback to Modern Flight Control Synthesis.* Springer-Verlag, 1982